Static and Dynamic Behavior of Saturation-Induced Saliencies and Their Effect on Carrier-Signal-Based Sensorless AC Drives

Fernando Briz, Michael W. Degner, *Member, IEEE*, Alberto Diez, and Robert D. Lorenz, *Fellow, IEEE*

***Abstract*—This paper analyzes the origin and the behavior of saturation-induced saliencies in induction machines, and their influence on carrier-signal-injection-based sensorless techniques. The modeling of saturation-induced saliencies is necessary for the estimation of flux position, while the minimization of their influence is desired for the estimation of rotor position. Specifically focusing on rotor position estimation, there are two ways to achieve this minimization, the first being the use of a machine design that reduces the magnitude of the undesired saturation-induced saliencies and the second being the compensation in the estimator of the undesired saturation-induced saliencies. The modeling of saturation-induced saliencies, not only statically, but also dynamically, i.e., when the operating point of the machine changes, will be addressed by this paper.**

***Index Terms*—Position estimation, saturation-induced saliencies, self sensing, sensorless control.**

I. Introduction

SENSORLESS operation of ac drives has been a field of intensive research during the past two decades. Although important advances have been made, and it is currently used in numerous industry applications, important limitations still exist that prevents its universal application.

It is now accepted that no single sensorless method is capable of controlling all types of machines or under all operating conditions. Techniques that rely on the back electromotive force (EMF) of the machine have been shown to be capable of providing high-performance field-oriented control in the medium- to high-speed range. As the speed decreases, and more specifically, the excitation frequency decreases, the parameter sensitivity of the methods becomes greater, and in the limit, they fail due to inobservability of the rotor quantities for dc excitation of the stator [1]–[3].

An alternative method, based on the tracking of saliencies by means of an injected carrier-signal excitation into the machine (voltage or current), has been recently proposed [4], [5]. This method has received a lot of attention from both academia and industry due to its capability of providing accurate high-bandwidth position and speed estimates, even at zero speed and frequency. Two important characteristics limiting the widespread use of this method for general-purpose induction machine drives are the lack of a significant saliency inherent to the machine design and the presence of parasitic saturation-induced saliencies, which are present in the machine for almost all levels of flux.

This paper analyzes and discusses the static and dynamic modeling of saturation-induced saliencies. The physical origin of such saliencies, their dynamic behavior under changing operating conditions, and the expected estimator performance with decoupling of the saturation-induced saliencies is covered.

II. Components of the Negative-Sequence Carrier-Signal Current

When a balanced polyphase carrier-signal voltage vector is applied to a salient machine, the resulting carrier-signal current vector can be used to estimate the position of the saliency [4], [5]. Although some types of machines, such as salient-pole or buried permanent-magnet synchronous machines, are deliberately designed to be salient, induction machines are designed and usually modeled as being nonsalient.

The assumption that induction machines are nonsalient is, in fact, rarely, if ever, true (the saliencies are typically very small and not including them in modeling is usually a very safe assumption). Saliencies exist in standard induction machine designs due to nonlinear magnetics (saturation-induced saliencies), even at very low flux levels, and due to the effects of rotor and stator slotting [4]–[16]. In addition, rotor-position-dependent saliencies can be created in several ways (deterministically opening the rotor slots in a spatial harmonic pattern [4], [3], [14]–[16], modulating the rotor bars resistance or depth [7], [10]) for the specific purpose of being tracked for rotor position estimation.

The simplest implementation of carrier-signal-based sensorless control is obtained when the spatial saliency present in the machine gives rise to a single harmonic in the negative-sequence carrier current [4], [5]. Additional harmonics are often created by the presence of other spatial inductance variations, or salien-

Paper IPCSD 02–007, presented at the 2001 Industry Applications Society Annual Meeting, Chicago, IL, September 30–October 5, and approved for publication in the IEEE TRANSACTIONS ON INDUSTRY APPLICATIONS by the Industrial Drives Committee of the IEEE Industry Applications Society. Manuscript submitted for review October 15, 2001 and released for publication March 6, 2002. This work was supported by the University of Oviedo, Ford Motor Company, and the Wisconsin Electric Machines and Power Electronics Consortium (WEMPEC), University of Wisconsin, Madison, and supported in part by the Research, Technological Development and Innovation Programs of the Principado of Asturias, under Grant PB-EXP01-24, and of the Spanish Ministry of Science and Technology-ERDF under Grant DPI2001-3815.

F. Briz and A. Diaz are with the Department of Electrical, Computer and Systems Engineering, University of Oviedo, E-33204 Gijón, Spain (e-mail: fernando@isa.uniovi.es; alberto@isa.uniovi.es).

M. W. Degner is with the Ford Research Laboratory, Ford Motor Company, Dearborn, MI 48121-2053 USA (e-mail: mdegner@ford.com).

R. D. Lorenz is with the Departments of Mechanical Engineering and Electrical and Computer Engineering, University of Wisconsin, Madison, WI 53706-1572 USA (e-mail: lorenz@engr.wisc.edu).

Publisher Item Identifier S 0093-9994(02)05014-4.

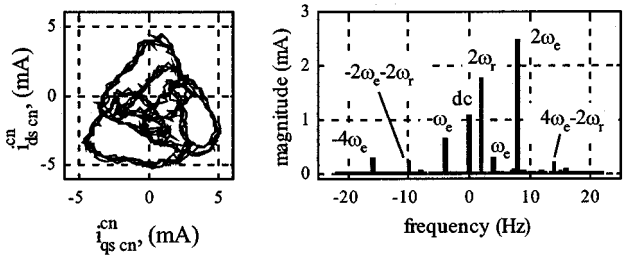

Fig. 1. Negative-sequence carrier-signal current trajectory and frequency spectrum in the negative-sequence carrier-signal reference frame with rated current and rated flux, $\omega_e = 4$ Hz and $\omega_r = 1$ Hz, using Motor #1 in Table I. A carrier voltage of $V_c = 7$ V and frequency of $\omega_c = 535$ Hz were used.

TABLE I
INDUCTION MOTORS PARAMETERS

	MOTOR #1	MOTOR #2
# Stator slots	24	24
# Rotor slots	30	30
Rotor slots type (prior to modification)	Skewed, closed	Skewed, closed
Engineered saliency period	Equal to the pole pitch	Equal to the pole pitch
Power rating	0.75 kW	0.9 kW
Poles	4	4
Rated current (rms)	2.1 A	2.4 A
Rated slip	2.83 Hz (85 rpm)	2.83 Hz (85 rpm)
R'_s	14.3 Ω	12.2 Ω
$L_{\sigma s}$	0.063 H	0.042 H
Rotor time constant τ_r	0.085 s	0.085 s

cies. Negative-sequence carrier-signal current components can also be caused by implementation issues, such as inverter dead-time or current switching harmonics, and not by actual saliencies in the machine.

Fig. 1 shows the negative-sequence carrier-signal current and the corresponding complex vector spectrum of a machine with an engineered rotor saliency operated at rated flux and rated load. From the figure, it can be seen that the frequency of all the relevant components in the spectrum near the negative-sequence carrier-signal frequency $-\omega_c$ are related to the electrical frequency, the rotor speed, or the combined effect of both. The harmonics can be categorized as follows.

1) The dc component corresponds to a stationary saliency. Unequal current sensor or amplifier gains and/or asymmetries in the machine are the most likely causes of this component.
2) The $\pm\omega_e$ harmonics have previously been reported and attributed to saturation [9], [13]. Some evidence exists that they are actually associated with switching harmonics and aliasing effects when sampling the phase currents [16].
3) The $2\omega_r$ harmonic is due to the engineered rotor saliency created by opening the rotor slots as stated in Table I.
4) Saturation-induced saliencies are the most likely source for the harmonics at 2, -4, 8, $\cdots$ ω_e, i.e., components of the negative-sequence carrier-signal current at frequencies defined by (1) in the negative-sequence carrier-signal reference frame

$$\omega^{cn}_{cn\,k} = 2\omega_e \cdot (1 \pm 3k), \qquad \text{with } k = 0, 1, 2, 3, \ldots. \quad (1)$$

For the case of $k = 0$, the primary saturation-induced harmonic is obtained, with a frequency $\omega^{cn}_{cn\,k} 2\omega_e$. In [13], it was shown that a potential explanation the rest of the harmonics is the saturation-induced saliency not having a sinusoidal spatial distribution and instead containing additional spatial harmonics, specifically even harmonics.
5) Finally, the interaction between the rotor saliency and the saturation-induced saliency give rise to an additional set of harmonics at frequencies defined by

$$\omega^{cn}_{cn\,k} = -2(\omega_r + \omega_e(1 \pm 3k)), \qquad \text{with } k = 0, 1, 2, 3, \ldots. \quad (2)$$

Although these harmonics have a relatively small magnitude, they can still affect the estimation accuracy.

The presence of any harmonics other than the desired harmonic (either rotor position dependent or the primary saturation induced) will cause estimation error unless they are substantially compensated for or decoupled. The magnitude of this error depends on the relative magnitude of the desired component versus the magnitude of the additional components that are within the estimation bandwidth.

For rotor position estimation, increasing the magnitude of the rotor-position-dependent saliency can reduce the estimation errors due to secondary saliencies. However, significant practical limitations exist. First, the modification of the rotor to create a saliency compromises at a certain level the fundamental operation of the machine, e.g., decreased torque capability, increased ripple torque, etc. Second, even when the rotor slots are opened following a sinusoidal pattern, secondary rotor-position-dependent harmonics can be created due to the discrete nature of the rotor slotting and nonlinear behavior of the machine. The presence and magnitude of these secondary harmonics becomes more severe as the rotor slot openings are made larger in an attempt to increase the magnitude of the primary harmonic.

III. STATIC MODELING OF SATURATION-INDUCED SALIENCIES

As stated in the previous section, only some of the components seen in the negative-sequence carrier-signal spectrum are believed to actually be caused by saturation-induced saliencies, and these will be the focus of this paper. Saturation-induced saliencies are expected to give rise to frequency components in the negative-sequence carrier-signal current at frequencies according to (1) [13]. Since stator windings are designed to accentuate the fundamental spatial components and to attenuate higher spatial harmonics, the most relevant saturation-induced saliency has a period equal to the pole pitch and rotates at twice the fundamental frequency, $2\omega_e$, in electrical degrees. Because of its relatively large magnitude, often bigger than the rotor-saliency-induced harmonic, compensation or decoupling of the $2\omega_e$ harmonic is necessary if reliable and accurate rotor position estimation is desired.

Modeling and measurement of saturation-induced saliencies has been analyzed in several previous works [5], [6], [9]–[13], with the reduction of their effects approached from two different perspectives: 1) the minimization of the saliencies through motor design practices [4] and 2) the decoupling of their associated negative-sequence carrier current using data

previously stored during a commissioning process [9], [10], [13].

Up to now, changes in the machine design to reduce the effects of saturation-induced saliencies have not been the focus of much research. One example of how saturation can be substantially reduced through machine design process is the presence of a minimum slot opening above each of the rotor bars [4].

When decoupling of saturation-induced saliencies is used understanding their physical origin is important. The stator leakage flux, rotor leakage flux, and air-gap flux all contribute, to some extent, to the overall saturation of the machine and, hence, to the presence of saturation-induced saliencies. Saturation-induced saliencies associated with the stator leakage flux are easier to compensate for since they depend on the magnitude and position of the stator current, which is measurable. Compensation of rotor leakage flux or air-gap-flux-dependent saturation-induced saliencies is more difficult since their magnitude and position are also dependent on the rotor current, which is not easily measurable.

The measurement of saturation-induced saliencies requires the determination of the magnitude and angle of the different negative-sequence carrier-signal harmonics under a steady-state condition. While the magnitude is easy to obtain, measurement of the angle requires the establishment of a reference axis. Although this might seem a relatively minor issue, it plays a major role in the implementation of decoupling methods for saturation-induced harmonics. Two different reference axes are commonly found in the literature: the stator current angle and the rotor flux angle.

Using the rotor flux angle as the reference angle has an advantage in that angle is usually used to implement field orientation and, therefore, variables that can play a significant role in the creation of saturation-induced saliencies are already referred to it. Since the rotor flux angle can not be measured, but needs to be estimated, this creates a problem when indirect field orientation or a current-model-based flux estimator or observer is used for the rotor flux estimation, as is commonly done for low excitation frequencies. This issue will be analyzed in an upcoming section.

Using the stator current angle, on the other hand, as the reference angle has the advantage that it is exactly known. Nevertheless, this is an advantage only if the stator current position plays a dominant role in determining the position of saturation-induced saliencies.

Fig. 2 shows the most significant components of the negative-sequence carrier-signal current, relative to the fundamental current, as a function of the slip frequency for Motor #1 in Table I, with constant rotor flux and the q-axis current varied according to the slip frequency. Although five different harmonics are shown, it is noted that only two of them, those at $2\omega_e$ and $-4\omega_e$ are believed to be due to saturation-induced saliencies. An interesting fact that can be seen from the figure is that the phase of the $2\omega_e$ component barely moves for the changes in working conditions. This result strongly suggests that the stator leakage flux is responsible for the saturation-induced saliency that causes this harmonic. It should be noted that for the case of slip $= 0$, i.e., $\omega_r = \omega_e$, the rotor-position-dependent harmonic at $2\omega_r$ and the saturation-induced harmonic at $2\omega_e$ coincide and are not distinguishable from each other; these points

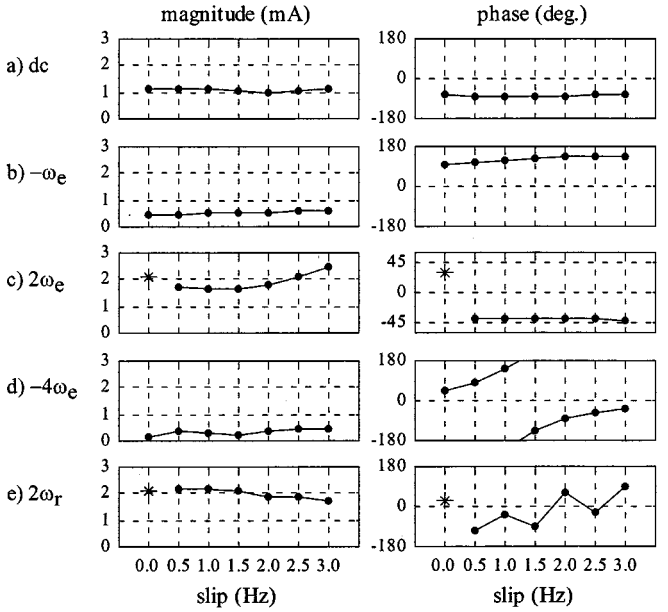

Fig. 2. Magnitude and phase, relative to the fundamental current, of the most significant negative-sequence harmonics as a function of the slip frequency for Motor #1 in Table I. The motor was operated at rated rotor flux with the q-axis current varied proportional to the slip. A constant fundamental excitation frequency $\omega_\rho = 4$ Hz was used, the rotor frequency was varied from $\omega_r = 4$ Hz (slip $= 0$ Hz) to 1 Hz (slip $= 3$ Hz). A carrier frequency of 535 Hz was used.

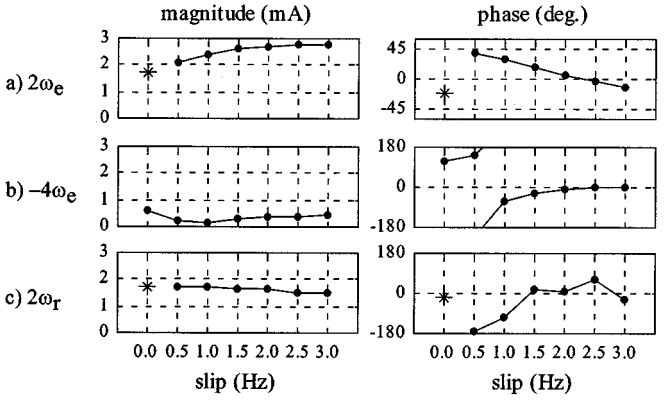

Fig. 3. Magnitude and phase, relative to the fundamental current, of the most significant negative sequence harmonics as a function of the slip frequency, for Motor #2 in Table I, operated under the same condition stated in Fig. 2.

are marked with an "$*$." It is also noted that the phase angle for the $2\omega_r$ harmonic, shown in Fig. 2(e), varies randomly for the different slips. This is expected since the rotor-position-dependent saliency and the stator current angle used as the reference angle are not related in any way.

Fig. 3 shows the same experiment for a machine from a different manufacturer, labeled as Motor #2 in Table I. Although apparently having a similar design, the behavior of the $2\omega_e$ harmonic is seen to be different, with its phase definitely moving as a function of the torque level. This suggests that other fluxes, in addition to the stator leakage flux, play a significant role in the creation of the saturation-induced saliency causing this harmonic. For this machine, the angle of the $2\omega_e$ harmonic changed roughly 45° from the no-load to the rated-load condition. Since the $2\omega_e$ harmonic rotates at twice the rate of the flux causing the saliency, this means that the position of the flux causing that

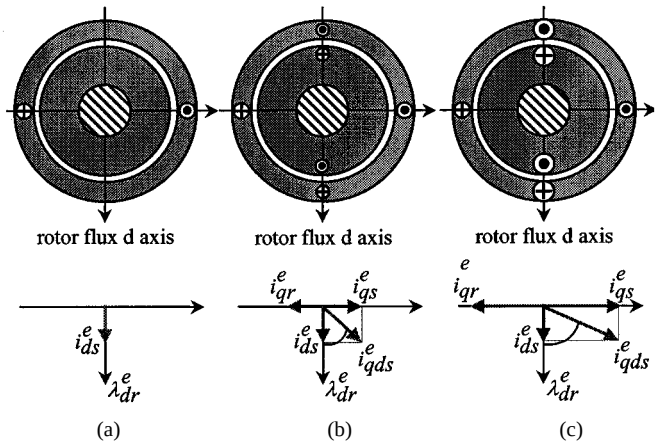

Fig. 4. Schematic representation of the relative position between the rotor flux and the stator current for the case of rated flux and three different levels of load, shown in a rotor-flux reference frame for a two-pole machine. (a) Rated flux, no load. (b) Rated flux, light load. (c) Rated flux, full load.

harmonic moved roughly 23° (in electrical units) as the q-axis current changed from zero to its rated value.

Additional insight into what flux, stator leakage, rotor leakage, or magnetizing actually causes saturation-induced saliencies can be gained by analyzing the relative position between the fluxes. Fig. 4 shows a schematic representation of the currents and rotor flux position for different load levels in a two-pole machine. It is noted that the current vectors are by definition located 90 electrical degrees from the maximum current-density location.

Saturation due to the stator leakage flux would be aligned with the maximum current-density spatial location. From Fig. 4(a), rated flux and no load, it is seen that the rotor flux and the stator current maximum density positions are located 90° from each other. This means that if both the rotor flux and the stator leakage flux were responsible to a similar degree for the saturation-induced harmonics, the resulting negative-sequence carrier-signal components would be 180° out of phase and would, therefore, compensate for each other. From the figure, it is also seen that, as the q-axis current is increased, the angle between the stator current and the rotor flux changes. The increase in that angle from no-load to rated-load condition depends on the ratio of rated q-axis current to rated d-axis current. This ratio changes with machine design, but it roughly varies from 45° for the case of small machines to more than 80° for the case of large machines. As a conclusion, if saturation-induced saliencies were mostly associated with the rotor flux, using the stator current angle as the reference angle would give rise to variations in the measured angle of the $2\omega_e$ component ranging roughly from 90° to 160°. On the other hand, similar variations should be expected if saturation-induced saliencies were mostly associated with the stator leakage flux and the rotor flux angle were used as the reference angle.

Using this theory, the experiments shown in Figs. 2 and 3 support the conclusion that the stator leakage flux plays a major role in the creation of saturation-induced saliencies for these two machines. Test conducted on other small machines, ranging from 0.75 up to 2.2 kW, from different manufacturers, showed similar results.

Comparing the results included in this paper for the position of $2\omega_e$ harmonic with the results from other researchers is not a straightforward task since a variety of practical issues including machine design, inverter operation (switching frequency, deadtime, etc.), filtering (phase lags due to antialiasing filters, digital filtering, etc.), A/D converter resolutions and digital signal processor (DSP) capability, among others, influence the results. Despite these considerations, some conclusions from the reported results can still be reached. The magnitude and the phase of the $2\omega_e$ harmonic relative to the rotor flux position have been reported in [9]–[11]. The measured magnitudes in [10] and [11] agree, relatively, with the results shown in Figs. 2(c) and 3(a), where the magnitude of the saliency increases with the fundamental current magnitude. The magnitude results reported in [9] are dramatically different. Concerning the phase variation of the $2\omega_e$ harmonic, the machine used in [11, Fig. 5(a)] behaved relatively similar to the results shown in Fig. 3(a) for Motor #2 in Table I. It is noted that in [11] the saliency position instead of the $2\omega_e$ component angle was plotted. The machines used in [9] and [10] appear to behave similar to Motor #2 in Table I whose results are shown in Fig. 3(a), i.e., the $2\omega_e$ component angle shows a relatively small shift when the load changes.

IV. Decoupling of Saturation-Induced Saliencies

A. Expected Performance of Decoupling

The compensation of saturation-induced saliencies using decoupling techniques has been proposed through the use of lookup tables, where the magnitude and phase of the most relevant saturation-induced negative-sequence carrier-signal current harmonics are stored under specific steady-state working conditions [9], [10], [13], errors in the estimated position after decoupling smaller than one mechanical degree have been reported [9], [10]. The overall robustness and accuracy of the resulting estimation depends on the accuracy of the compensation and will be influenced by the magnitude and harmonic order of the rotor saliency, the number and magnitude (relative to the magnitude of the rotor saliency) of the relevant saturation-induced harmonics, and the accuracy in the modeling (both magnitude and phase) of saturation-induced saliencies that are decoupled.

Equation (3) shows the instantaneous position estimation error for the case of a machine with a rotor saliency when a single saturation-induced harmonic also exists and is decoupled

$$\theta_r - \hat{\theta}_r = \frac{1}{h_1}\angle\left(I_{cn1} + I_{cn2}e^{j(h2\theta_e - h_1\theta_r + \phi_2)} - \hat{I}_{cn2}e^{j(h2\hat{\theta}_e - h_1\theta_r + \hat{\phi}_2)}\right) \quad (3)$$

where $\angle$ denotes taking the angle of the resulting complex vector, θ_r and $\hat{\theta}_r$ are the actual and estimated rotor position in mechanical degrees, I_{cn1} and h_1 are the magnitude and the harmonic order of the rotor position harmonic in mechanical degrees, respectively, I_{cn2} and $\hat{I}_{cn2}$ are the actual and estimated saturation-induced harmonic magnitudes, respectively, h_2 is the harmonic order of the saturation-induced harmonic in mechanical degrees, θ_e and $\hat{\theta}_e$ are the actual and estimated positions of the saturation-induced saliency, respectively, in

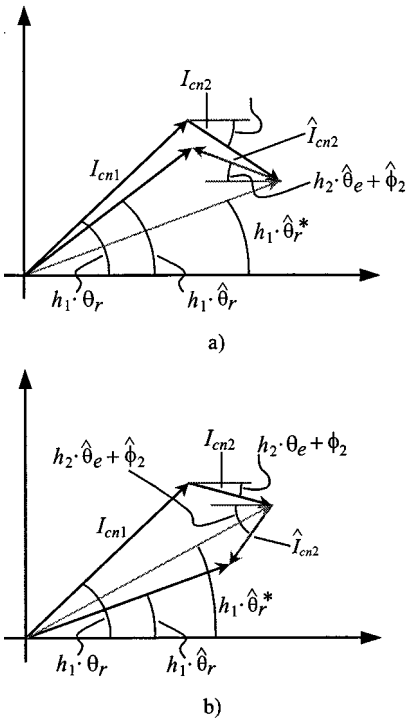

Fig. 5. Estimation error resulting from inexact decoupling of a secondary harmonic. (a) Secondary harmonic with a small error in the decoupling angle. (b) Secondary harmonic with a large error in the decoupling angle.

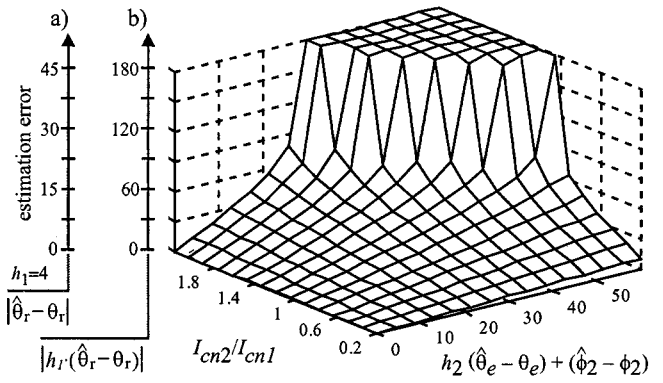

Fig. 6. Maximum rotor position estimation error in mechanical degrees as a function of the relative magnitude of the negative-sequence carrier-signal current induced by the rotor saliency and the secondary saliency, I_{cn1} and I_{cn2}, respectively, and the estimation error in the secondary saliency decoupling angle, for the case of a machine with $p = 4$ and $h_1 = 4$.

mechanical degrees, and $\hat{\phi}_2$ and ϕ_2 are the estimated and actual phase shift of the saturation-induced component of the negative-sequence carrier-signal current relative to the position of the saliency.

Fig. 5(a) shows a graphic representation of (3) and the improvement in the estimated rotor position with respect to the case of the saturation-induced saliency not being decoupled (labeled as $\hat{\theta}_r^*$). The maximum rotor position estimation error as a function of the saturation-induced harmonic estimation error can be obtained by evaluating (3) at its maximums. Fig. 6 shows the maximum of (3) obtained by numerically solving the equation for the case of $I_{cn2} = \hat{I}_{cn2}$, i.e., no estimation error in the saturation-induced harmonic magnitude. This assumption was included to simplify the analysis and will never be exactly true in practice. The solution was calculated as a function of the estimation error in the saturation-induced harmonic position and the relative magnitude of the saturation-induced harmonic with respect to the rotor position harmonic. Some interesting conclusions can be obtained from (3) and Fig. 6.

- Decoupling of a harmonic will decrease the maximum rotor position estimation error only when the decoupling angle ($h_2\hat{\theta}_e+\hat{\phi}_2$) error is limited. For the case considered, with no error in the decoupled saliency magnitude, this error limit would be 60°. For estimation errors in angle larger than 60°, decoupling would actually increase the maximum rotor position estimation error with respect to the case of no decoupling. An example of this is shown in Fig. 5(b).
- From Fig. 6, it can be seen that for the case of a saliency period equal to the pole pitch *a),* the maximum estimation error is 45 mechanical degrees. This does not mean that the maximum estimation error cannot go beyond that limit, but that if it does the estimated position will jump to the next stable operating point, $360/h_1$ mechanical degrees away (90° for the case of a four-pole machine and a rotor saliency that rotates at the same speed as the rotor). This jump will cause a transient disturbance in the estimation of the rotor flux position, resulting in the momentary loss of field orientation. The effects of such a jump on motion control depend on the application but they would be expected to be more severe.
- The number of harmonics that need to be decoupled as a function of the desired accuracy in the estimated position can also be addressed using similar techniques to those used to create Fig. 6. Nevertheless, the decoupling of any harmonic will first require an assessment of how accurately it can be modeled, both in magnitude and phase.

Saturation-induced harmonics whose phase is closely related to the stator current angle (and, therefore, likely caused in some aspect by the stator leakage flux) can be mapped and decoupled with a relatively high accuracy. On the other hand, harmonics closely related to any of the other fundamental excitation fluxes are more to difficult decouple. It is noted that these harmonics can be accurately mapped during a commissioning process if a position sensor is used in conjunction with a flux observer to estimate the flux position. Even so, the coupling between the flux angle estimation and the decoupling of the secondary saliencies is a major source for error under sensorless operation.

B. Rotor Position Estimation and Flux Angle Estimation

Analyzing the coupling between flux angle estimation and rotor position estimation when saturation-induced saliencies are dependent on the air-gap flux or rotor leakage flux (i.e., fluxes whose position cannot be measured) is not easy. The flux angle estimation necessary for field orientation will use either a flux estimator or observer, which will have some error in its parameters. The resulting error in the flux angle estimate will cause errors in the decoupling of saturation-induced harmonics. Alternatively, errors in the model of the saturation-induced harmonics would cause similar behavior. Because of this, it is difficult to distinguish between, if even possible, the errors in decoupling

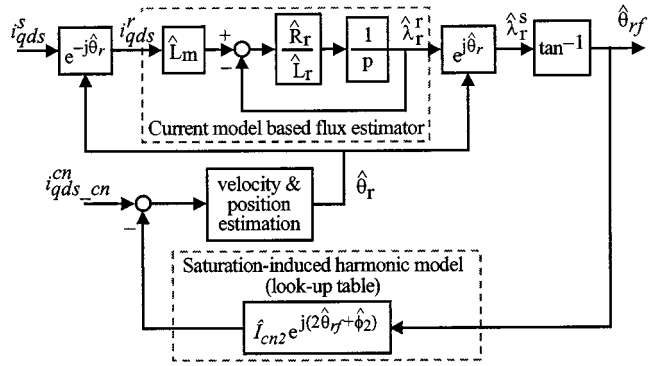

Fig. 7. Rotor flux angle estimation using a current-model-based flux estimator (shown in a rotor position synchronous reference frame) and decoupling of a saturation-induced harmonic dependent on the rotor flux position. The machine has a rotor-position-dependent saliency and a saturation-induced saliency, both with a harmonic order h equal to the pole number.

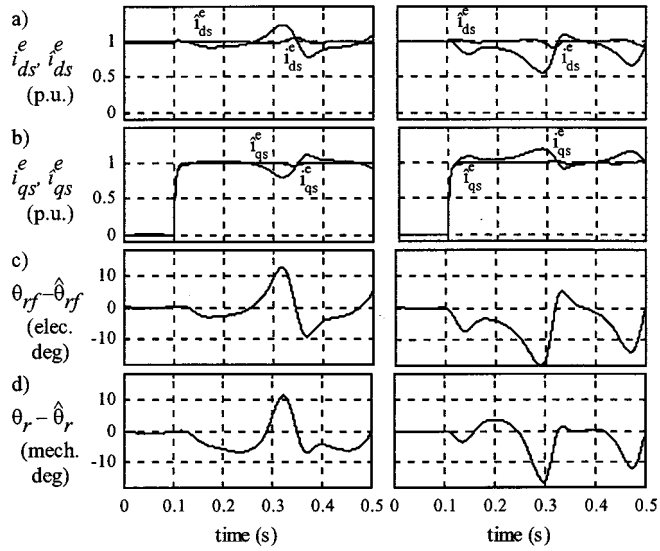

Fig. 8. Simulated field-oriented control and position estimation of a machine with its rotor locked, using a current-model-based flux estimate with (a) no error in its parameters but a 10 electrical degrees error in the decoupling angle of the saturation-induced harmonic and (b) a 20% estimation error in the flux observer rotor resistance and no error in the decoupling angle of the saturation-induced harmonic.

that are being caused by an incorrect flux angle estimate from those due to an incorrect model of the saturation-induced harmonics.

To gain some insight into this problem, a simulation of a sensorless-controlled field-oriented induction machine was conducted, with the results shown in Fig. 8. A current-model-based flux estimator, as shown in Fig. 7, was used to estimate the rotor flux angle. The saturation-induced saliency was modeled as being dependent on the rotor flux position. For the first case shown in Fig. 8(a), exact parameter estimates were used in the flux estimator, while an error of 10 electrical degrees in the angle modeling the saturation-induced saliency harmonic $2\hat{\theta}_{rf}+\hat{\phi}_2$ existed. Because of this error, the decoupling of the saturation-induced saliency was incorrect, which then influenced the rotor position estimation. From Fig. 8(a) it is seen that despite the correct parameters of the flux estimator, error in the estimation of $\hat{\theta}_r$ caused estimation errors in the rotor flux angle $\hat{\theta}_{rf}$, affecting field orientation and also the decoupling of the saturation-induced harmonic.

If errors in the flux estimator parameters exist, a similar process will occur, even if the saturation harmonic had been correctly modeled during the commissioning process. This is shown in Fig. 8(b), where an exact model for the saturation-induced harmonic is used, but a 20% error in the rotor resistance estimate used in the rotor flux estimator exists.

In practice, errors would always be expected to exist in both the machine parameters for the flux angle estimator and in the saturation-induced harmonic model. The presence of the coupling between flux angle estimation and rotor position estimation depends on whether the saturation-induced harmonics can be modeled as a function of measurable variables, e.g., the stator current, or are dependent on an estimated flux angle.

C. Suitability of an Induction Machine for Sensorless Operation

Fig. 9 shows the variation in the magnitude and phase of the $2\omega_e$ and $-4\omega_e$ negative-sequence harmonics for the fundamental current varying from the no-load to approximately rated-load condition and the slip frequency varying from zero to approximately its rated value using Motor #1 in Table I. The $2\omega_e$ negative-sequence harmonics are not shown for the case of zero slip, since for that case it coincides with the harmonic due to the engineered rotor saliency. It is noted that the machine was not operated using field-oriented control. The goal of the experiment was to gain insight into how severe the coupling can be between the position estimation and the decoupling of the saturation-induced harmonics.

Any major variation of a saturation-induced harmonic (either magnitude or phase) as a function of the fundamental current level (for constant slip) is not expected to be a major cause of errors in the decoupling since the fundamental current is a measured quantity. On the other hand, any variation of a saturation-induced harmonic as a function of the slip frequency (for constant fundamental current level) can lead to difficulty in minimizing estimation errors. This is because decoupling of these harmonics is dependent on having an accurate knowledge of the slip (field position), which, as shown in the previous section, is in turn dependent on the estimated rotor position, the quantity that the decoupling is attempting to improve.

Machines with minimal saturation-induced harmonics or ones that have a reduced dependency of saturation-induced harmonics on the slip frequency would show the most promise. Specifically, for the machine shown in Fig. 9, it is seen that the $2\omega_e$ component can accurately be decoupled since its magnitude and phase has a low dependence on the slip frequency. Opposite to this, the variation of the $-4\omega_e$ harmonic, mainly its phase, is seen to be strongly dependent on the slip frequency. Accurate decoupling of this component is expected to be more problematic.

Similar experiments to that shown in Fig. 9 were performed on machines with similar power ratings (verification of these conclusions for larger machines is still needed); from these experiments, some general conclusion can be made.

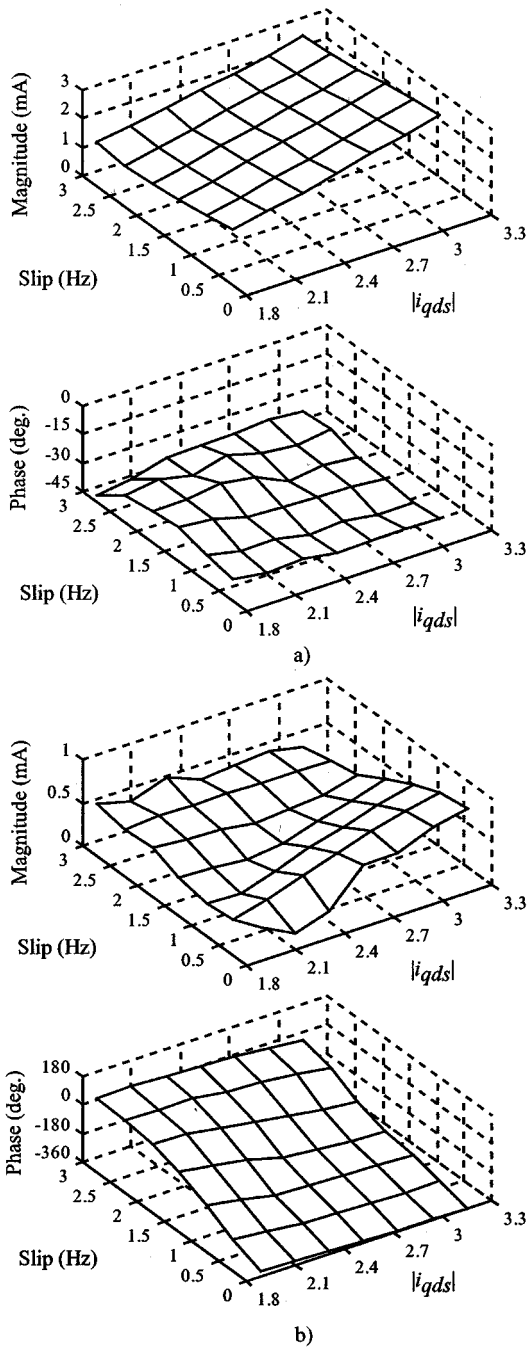

Fig. 9. Magnitude and phase (relative to the fundamental current) of the (a) $2\omega_e$ and (b) $-4\omega_e$ fundamental-excitation-dependent negative-sequence harmonics as a function of the slip frequency and fundamental current level, for Motor #1 in Table I. A constant fundamental excitation frequency $\omega_e = 4$ Hz was used, with the rotor speed varied according to the slip shown in the figure. A carrier frequency of 535 Hz was used.

- The variation in the magnitude and phase of a particular harmonic as a function of the stator current and slip frequency are usually smooth and, therefore, suitable to be stored in a lookup table. Any discontinuities seen in these variations are usually caused by the interaction with other harmonics, not by a sudden variation in a specific harmonic. An example of this is the $2\omega_e$ harmonic in Figs. 2 and 3, which is corrupted by the $2\omega_r$ component for the case of zero slip.

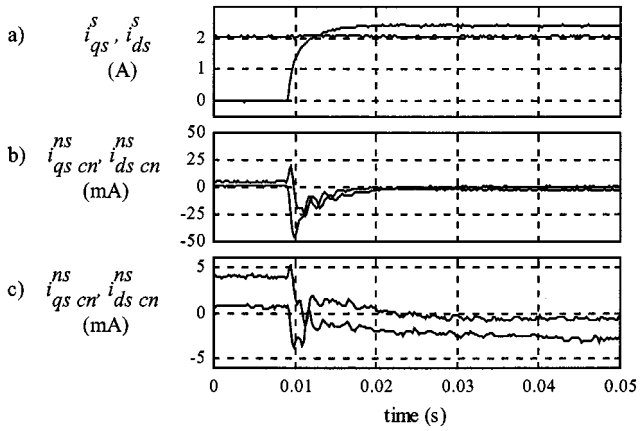

Fig. 10. Experimental results showing (a) dynamic response of the q-axis current in a stationary reference frame, with the d-axis current kept constant and the rotor locked, (b) q and d components of the negative carrier-signal current during the transient in the fundamental current, and (c) q and d components of the negative carrier-signal current during the transient in the fundamental current, with the fundamental current decoupled by means of a fundamental current observer. Motor #1 with a 100-Hz bandwidth current regulator was used.

- The $2\omega_e$ harmonic was always found to be highly dependent on the stator current vector. Nevertheless, the results were not always as good as the results for Motor #1, shown in Fig. 9.

Higher order harmonics were systematically found to have a higher rate of variation as a function of the operating point. Therefore, it is expected that the decoupling of saturation-induced harmonics will be more sensitive to the accuracy of the harmonic model/lookup table as their order increases.

V. Dynamic Behavior of Saturation-Induced Saliencies

The lookup tables necessary for the implementation of the compensation technique analyzed in the previous sections were measured under specific steady-state working conditions [9], [10], [13]. Although these lookup tables can be effective in decoupling saturation-induced saliencies during steady-state operation, it is not clear how changes in the fluxes causing the saturation-induced saliencies should be handled.

Before analyzing the dynamics of saturation-induced saliencies, it is important to consider other effects influencing the negative-sequence carrier-signal current during the transient operation of the machine and, specifically, those coming from the transients in the fundamental current. Fig. 10 shows the q and d components of the negative-sequence carrier-signal current when a step variation is commanded in the stationary frame q-axis fundamental current. The transient in the fundamental current produces a large amount of content spread across the frequency spectrum, some of which coincides with the actual negative-sequence carrier-signal current. The magnitude of these components can be more than a full order of magnitude larger than the actual negative carrier-signal current, as shown in Fig. 10(b), usually producing an inadmissible disturbance to the negative-sequence carrier-signal current. Despite their noticeable magnitude, these components are easily decoupled using a fundamental current observer [14]. Once these components have been decoupled [Fig. 10(c)], any variation in the

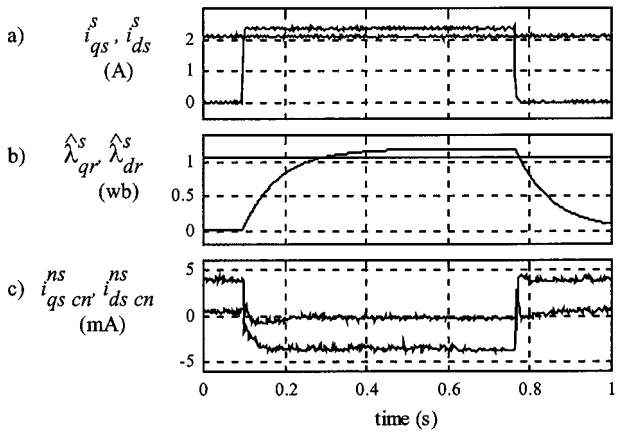

Fig. 11. Experimental results showing (a) dynamic response of the q-axis current in a stationary reference frame, with the d-axis current kept constant, and the rotor locked, (b) estimated rotor flux in a stationary reference frame, and (c) q and d components of the negative carrier-signal current during the transient in the fundamental current, with the fundamental current decoupled by means of a fundamental current observer.

negative-sequence carrier-signal current is due to saturation-induced saliencies or changes in the rotor-position-dependent saliency with current or flux level.

Fig. 11(c) shows the negative-sequence carrier-signal current when the fundamental current changes as shown in Fig. 11(a). It is noted that only current regulation was implemented, without field-oriented control, with the q- and d-axes quantities shown in a stationary reference frame. Fig. 11(b) shows the estimated rotor flux. Since the flux response is dominated by the rotor time constant, which is relatively large, its dynamics are definitely slower than those of the stator current. Even though all the fluxes present in the machine are expected to influence at a certain level the negative-sequence carrier-signal current, the fast dynamics of the negative-sequence carrier-signal current observed in Fig. 11(c) suggest that they are dominated by fast-changing leakage fluxes rather than by the slowly changing magnetizing flux. This, again, supports the conclusion that stator leakage flux is a major contributor to the saturation-induced harmonics in the negative-sequence carrier signal.

VI. Conclusions

The static and dynamic behavior of saturation-induced saliencies and the potential performance of carrier-signal-injection-based sensorless techniques with the presence of secondary parasitic saturation-induced harmonics has been analyzed in this paper. From this analysis, the following conclusions have been reached.

- In the machines tested, the stator leakage flux was been found to be responsible for a majority of the saturation-induced harmonics. Even so, the magnetizing flux was also found to be a contributor, with the degree of influence varying from machine to machine.
- The mutual dependence between rotor position estimation and field orientation can be a limiting factor for decoupling of the saturation-induced harmonics. This interdependence increases as the influence of the magnetizing flux in the creation of the saturation-induced saliencies increases.
- A testing procedure to evaluate the suitability of different machine designs for use in carrier-signal-injection-based sensorless applications has been established.

References

[1] H. Tajima and Y. Hori, "Speed sensorless filed orientation control of the induction machine," *IEEE Trans. Ind. Applicat.*, vol. 29, pp. 175–180, Jan./Feb. 1993.

[2] H. Kubota and K. Matsuse, "The improvement of performance at low speed by offset compensation of stator voltage in sensorless vector controlled induction machines," in *Conf. Rec. IEEE-IAS Annu. Meeting*, San Diego, CA, Oct. 1996, pp. 257–261.

[3] C. Schauder, "Adaptive speed identification for vector control of induction motors without rotational transducers," *IEEE Trans. Ind. Applicat.*, vol. 28, pp. 1054–1061, Sept./Oct. 1992.

[4] P. L. Jansen and R. D. Lorenz, "Transducerless position and velocity estimation in induction and salient ac machines," *IEEE Trans. Ind. Applicat.*, vol. 31, pp. 240–247, Mar./Apr. 1995.

[5] ——, "Transducerless field orientation concepts employing saturation-induced saliencies in induction machines," *IEEE Trans. Ind. Applicat.*, vol. 32, pp. 1380–1393, Nov./Dec. 1996.

[6] J. Ha and S. K. Sul, "Sensorless field orientation control of an induction machine by high frequency signal injection," in *Conf. Rec. IEEE-IAS Annu. Meeting*, New Orleans, LA, Oct. 1997, pp. 426–432.

[7] J. Cilia, G. M. Asher, and K. G. Bradley, "Sensorless position detection for vector controlled induction motor drives using an asymmetric outer-section cage," in *Conf. Rec. IEEE-IAS Annu. Meeting*, San Diego, CA, Oct. 1996, pp. 286–292.

[8] M. W. Degner and R. D. Lorenz, "Position estimation in induction machines utilizing rotor bar slot harmonics and carrier frequency signal injection," *IEEE Trans. Ind. Applicat.*, vol. 36, pp. 736–742, May/June 2000.

[9] N. Teske, G. M. Asher, M. Sumner, and K. J. Bradley, "Sensorless position estimation for symmetric cage induction motor under loaded conditions," in *Conf. Rec. IEEE-IAS Annu. Meeting*, Rome, Italy, Oct. 2000, CD-ROM.

[10] ——, "Suppression of saturation saliency effects for the sensorless position control of induction motor drives under loaded conditions," *IEEE Trans. Ind. Electron.*, vol. 47, pp. 1142–1150, Sept./Oct. 2000.

[11] M. L. Aime, M. W. Degner, N. Tice, and R. D. Lorenz, "The effects of saturation on flux angle estimation for sensorless, direct field oriented control of induction machines," in *Proc. EPE'99*, Lausanne, Switzerland, 1999, CD-ROM.

[12] M. L. Aime, M. W. Degner, and R. D. Lorenz, "Saturation measurements in AC machines using carrier signal injection," in *Conf. Rec. IEEE-IAS Annu. Meeting*, St. Louis, MO, Oct. 1998, pp. 159–166.

[13] F. Briz, A. Diez, M. W. Degner, and R. D. Lorenz, "Measuring, modeling and decoupling of saturation-induced saliencies in carrier-signal injection based sensorless AC drives," *IEEE Trans. Ind. Applicat.*, vol. 37, pp. 1356–1364, Sept./Oct. 2001.

[14] F. Briz, A. Diez, and M. W. Degner, "Dynamic operation of carrier signal injection based, sensorless, direct field oriented AC drives," *IEEE Trans. Ind. Applicat.*, vol. 36, pp. 1360–1368, Sept./Oct. 2000.

[15] M. W. Degner and R. D. Lorenz, "Using multiple saliencies for the estimation of flux, position, and velocity in AC machines," *IEEE Trans. Ind. Applicat.*, vol. 34, pp. 1097–1104, Sept./Oct. 1998.

[16] F. Briz, M. W. Degner, A. Diez, and R. D. Lorenz, "Implementation issues affecting the performance of carrier signal injection based sensorless controlled AC drives," in *Conf. Rec. IEEE-IAS Annu. Meeting*, Chicago, Sept. 30–Oct. 5, 2001, CD-ROM.

Fernando Briz received the M.S. and Ph.D. degrees from the University of Oviedo, Gijón, Spain, in 1990 and 1996, respectively.

From June 1996 to March 1997, he was a Visiting Researcher at the University of Wisconsin, Madison. He is currently an Associate Professor in the Electrical Engineering Department, University of Oviedo. His topics of interest include control systems, high-performance ac drives control, sensorless control, and digital signal processing.

Prof. Briz received a Prize Paper Award from the Industrial Power Converter Committee of the IEEE Industry Applications Society.

Michael W. Degner (S'95–A'98–M'99) received the B.S., M.S., and Ph.D. degrees in mechanical engineering from the University of Wisconsin, Madison, in 1991, 1993, and 1998, respectively, with a focus on electric machines, power electronics, and control systems.

He is currently with the Ford Research Laboratory, Ford Motor Company, Dearborn, MI, where his research is focused on the use of power electronics in automobile applications. His interests include control systems, machine drives, electric machines, power electronics, and mechatronics.

Alberto Diez received the M.S. and Ph.D. degrees from the University of Oviedo, Gijón, Spain, in 1983 and 1988, respectively.

He is currently an Associate Professor in the Electrical Engineering Department, University of Oviedo. In October 1998, he was nominated as a Member of the Executive Committee D2 "Rolling-flat products" by the European Commission. His topics of interest include control systems, high-performance ac drives control and industrial automation processes.

Robert D. Lorenz (S'83–M'84–SM'91–F'98)) received the B.S., M.S., and Ph.D. degrees from the University of Wisconsin, Madison, and the M.B.A. degree from the University of Rochester, Rochester, NY.

Since 1984, he has been a member of the faculty of the University of Wisconsin, Madison, where he is the Mead Witter Foundation Consolidated Papers Professor of Controls Engineering in both the Department of Mechanical Engineering and the Department of Electrical and Computer Engineering. He is Co-Director of the Wisconsin Electric Machines and Power Electronics Consortium, which celebrated its 20th anniversary in 2001. It is the largest industrial research consortium on motor drives in the world. He is also the thrust leader for control and sensor integration in the Center for Power Electronic Systems, an NSF Engineering Research Center (ERC) which is a joint ERC with Virgina Polytechnic Institute and State University, Rensselaer Polytechnic Institute, University of Puerto Rico-Mayaguez, and North Carolina A&T. From 1972 to 1982, he was a member of the research staff at the Gleason Works, Rochester, NY, working principally on high-performance drives and synchronized motion control. He was a Visiting Research Professor in the Electrical Drives Group, Catholic University of Leuven, Leuven, Belgium, in the summer of 1989 and in the Power Electronics and Electrical Drives Institute, Technical University of Aachen, Aachen, Germany, in the summers of 1987, 1991, 1995, 1997, and 1999, where he also was the SEW Eurodrive Guest Professor from September 1, 2000 until July 7, 2001. In 1969–1970, he conducted Master thesis research in adaptive control of machine tools at the Technical University of Aachen. His current research interests include sensorless electromagnetic motor/actuator technologies, real-time signal processing and estimation techniques, precision multiaxis motion control, and ac/dc drive and high-precision machine control technologies. He has authored more than 160 published technical papers and is the holder of more than 15 patents, with five more pending.

Dr. Lorenz was the IEEE Industry Applications Society (IAS) President for 2001, a Distinguished Lecturer of the IAS for 2000/2001, immediate past Chair of the IAS Awards Department, and past Chairman of the IAS Industrial Drives Committee, and is a member of the IAS Industrial Drives, Electric Machines, Industrial Power Converter, and Industrial Automation and Control Committees. He is also the current Chair of the Periodicals Committee for the IEEE Technical Activities Board. He is a member of the IEEE Sensor Council AdCom and the IEEE Neural Network AdCom. He is a Registered Professional Engineer in the States of New York and Wisconsin. He is also a member of the American Society of Mechanical Engineers, Instrument Society of America, and Society of Photo-Optical Instrumentation Engineers. He has won 13 prize paper awards.